


Molecular basis for the interaction between *Saccharomyces cerevisiae* Rtt103 and the Rat1-Rai1 complex

Received: 13 October 2024

Hsu-Feng Chu & Liang Tong  

Accepted: 25 March 2025

Published online: 05 April 2025

 Check for updates

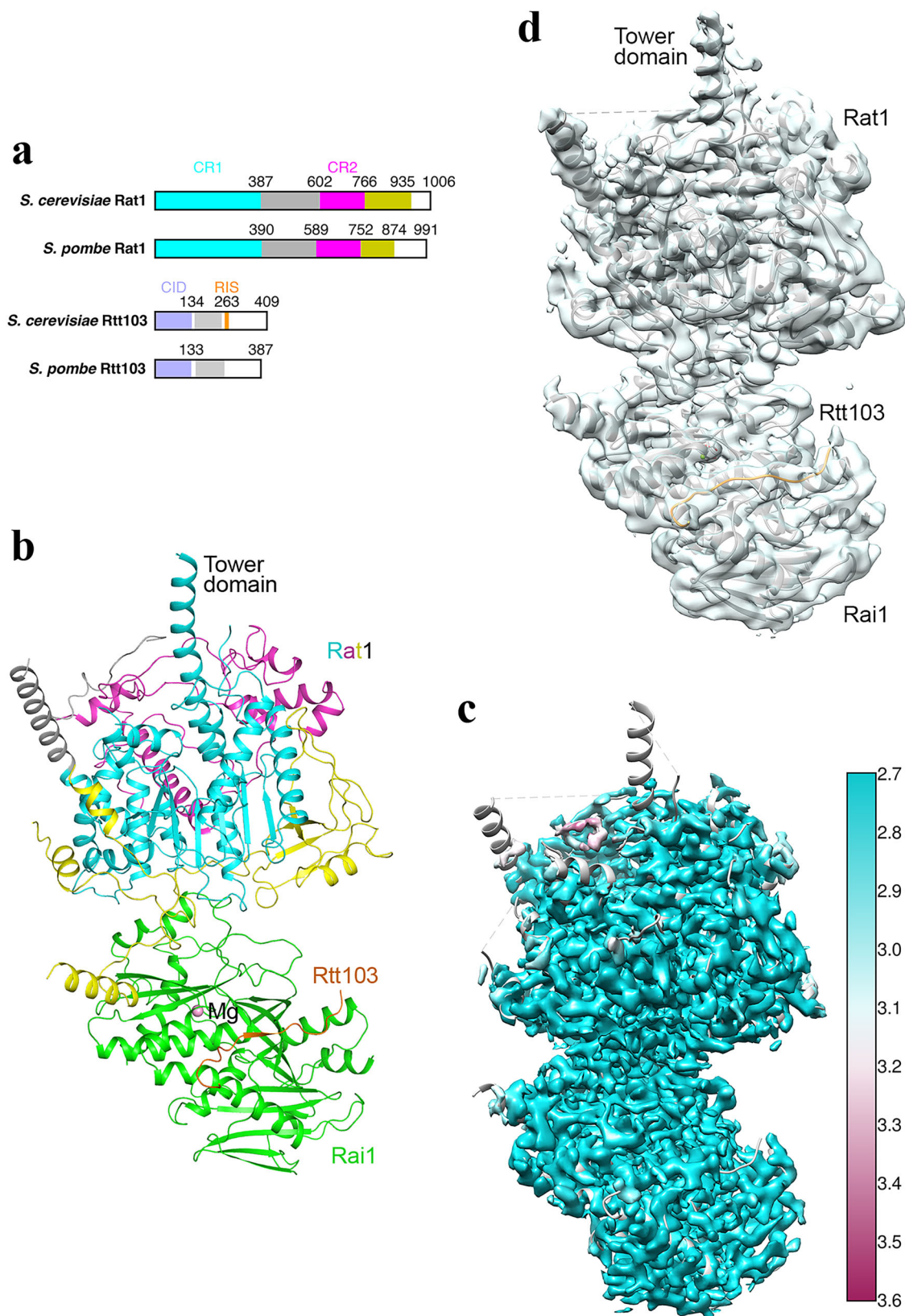
The Rat1 5'-3' exoribonuclease together with its partner Rai1 have important roles in *Saccharomyces cerevisiae* RNA polymerase II transcription termination. Rtt103 copurifies with Rat1-Rai1 in *S. cerevisiae*, but its mechanism of interaction with them is not known. We report here the cryo-EM structure of the *S. cerevisiae* Rat1-Rai1-Rtt103 ternary complex at 2.9 Å resolution. We found that a short segment of Rtt103 is in close contact with Rai1, while the rest of Rtt103, including its RNA polymerase II C-terminal domain interaction domain, shows no interactions with Rai1 or Rat1. This is in contrast to the observations on the *Komagataella phaffii* Rat1-Rai1-Rtt103 complex, where only the RNA polymerase II C-terminal domain interaction domain of Rtt103 has contacts with Rai1. Our structure reveals that *S. cerevisiae* Rtt103 Pro261 and Tyr263 have important contacts with Rai1, and we show that the P261G/Y263A mutation of Rtt103 blocks the interaction with Rat1-Rai1. Our structure suggests that, in yeast, this segment of Rtt103, which we have named the Rai1 interaction segment, likely helps the recruitment of Rat1-Rai1 to RNA polymerase II for termination.

The 5'→3' exoribonucleases (XRN) have important functions in RNA metabolism, including maturation of ribosomal and small nucleolar RNAs, RNA degradation, nonsense mediated decay, and other RNA quality control mechanisms. These enzymes require a 5' monophosphate on the RNA substrate, and therefore they are only active toward a defined subset of RNA species in the cell.

XRN2 (Rat1 in yeast) is also essential for the torpedo or unified model of transcription termination by RNA polymerase II (Pol II)^{1,2}. After cleavage of the Pol II transcript by the pre-mRNA 3'-end processing machinery, XRN2/Rat1 degrades the downstream cleavage product (which carries a 5' monophosphate), catches up to the polymerase and helps to displace it from the template^{3–6}. Rat1 functions together with the binding partner Rai1, which can stimulate its exonuclease activity^{7,8}. Rai1 and its mammalian homolog DXO also have decapping activity toward the 5' cap and capping intermediates as well as various non-canonical caps^{9–13}. The RNA products of Rai1/DXO contain a 5' monophosphate, enabling their degradation by the XRN, and some Rai1/DXO enzymes also possess distributive 5'-3' exoribonuclease activity^{11,14}.

The amino acid sequences of Rat1 and XRN contain two conserved regions (CR1 and CR2) at the N terminus, which are connected by a poorly conserved segment of variable length (Fig. 1a). A segment directly following CR2, though poorly conserved, has close contacts with CR1, and more importantly, this segment in Rat1 mediates the formation of the Rat1-Rai1 complex⁹. Recent structures of Rat1-Rai1 in complex with Pol II have provided molecular insights into how Rat1 interacts with Pol II and contributes to termination^{15,16}.

The Rat1-Rai1 complex was found to copurify with Rtt103 in *Saccharomyces cerevisiae*, and synthetic lethality was observed with the deletion of both Rtt103 and Rai1¹. While Rat1 and Rai1 have strong effects on Pol II termination, Rtt103 has a weaker contribution to this termination in *S. cerevisiae*. Rtt103 may also be involved in DNA damage response¹⁷, and Rtt103 deletion, as well as Rai1 deletion, leads to higher levels of sub-telomeric transcripts¹⁸. These transcripts are normally degraded, likely by Rat1, suggesting that Rtt103 may help to recruit the exonuclease for degradation. How Rtt103 interacts with the Rat1-Rai1 complex in *S. cerevisiae* was not known.



Rtt103 contains a Pol II CTD interaction domain (CID) at the N terminus^{1,19–22}, which is connected to a helical region by a short linker (Fig. 1a). The rest of the protein is poorly conserved among its homologs and does not appear to contain any secondary structures.

We report here the cryo-EM structure of the *S. cerevisiae* Rat1-Rai1-Rtt103 ternary complex at 2.9 Å resolution. We found that a short

segment of Rtt103 of about 10 amino acid residues just after the helical region is in close contact with Rai1, while the rest of Rtt103, including the CID, shows no interactions with Rai1 or Rat1. This is in sharp contrast to the observations on the *Komagataella phaffii* Rat1-Rai1-Rtt103 complex¹⁶, where only the CID of Rtt103 has contacts with Rai1. Our structure reveals that *S. cerevisiae* Rtt103 Pro261 and Tyr263 have

Fig. 1 | Structure of the *S. cerevisiae* Rat1-Rail-Rtt103 ternary complex. **a** Domain organization of *S. cerevisiae* and *S. pombe* Rat1 and Rtt103. Conserved region 1 (CR1) of Rat1 is colored in cyan, CR2 in magenta, and the linker between them in gray. A poorly conserved segment following CR2 that is also observed in our structure is in yellow. The CTD interaction domain (CID) of Rtt103 is in light blue, and a helical region in gray. The Rail interaction segment (RIS) of *S. cerevisiae* Rtt103 is in orange. **b** Schematic drawing of the structure of *S. cerevisiae* Rat1-Rail-Rtt103 ternary complex. Residues are colored according to panel (a). A putative metal ion in the

active site of Rail is shown as a sphere (pink). **c** EM density of the Rat1-Rail-Rtt103 complex colored by local resolution. The atomic model is also shown, and several segments on the surface have no EM density in this final map. **d** EM density of the Rat1-Rail-Rtt103 complex after a heterogeneous refinement. Density is observed for several segments on the surface. All the structure figures were produced with PyMOL (www.pymol.org) unless otherwise noted. Panels **c** and **d** were produced with UCSF Chimera²⁸.

important contacts with Rail. We introduced mutations at these residues and showed that they blocked the interaction with Rat1-Rail, confirming the structural observations. Our structure suggests that this segment of Rtt103, which we have named the Rail interaction segment (RIS), likely helps the recruitment of Rat1-Rail to Pol II for termination.

Results and discussion

Overall structure of Rat1-Rail-Rtt103 ternary complex

To produce the Rat1-Rail-Rtt103 complex, we first tried to express the three proteins separately in *E. coli* and assemble them in vitro. Although Rat1 and Rtt103 could be expressed and purified, Rail was prone to aggregation during purification, potentially due to misfolding. We then co-expressed the three proteins in insect cells and were able to purify the ternary complex.

The structure of the *S. cerevisiae* Rat1-Rail-Rtt103 ternary complex has been determined by cryo-EM at 2.9 Å resolution (Fig. 1b, c, Table 1, Supplementary Fig. 1). Much of the linker between CR1 and CR2 and

several loops on the surface of Rat1 have no density in the final EM map (Fig. 1c). However, EM density is visible for some of these residues in the map after heterogeneous refinement (Fig. 1d), including the tower domain helix, and the residues are included in the atomic model, although they have poor fit to the final EM density, as indicated in the validation report.

Rail is bound to the opposite face from the active site of Rat1, generally in the same location as observed in the *S. pombe* Rat1-Rail complex (see below)⁹. EM density was observed at the binding site of one of the metal ions in the active site of Rail⁹, and a magnesium ion is placed at this position, although divalent metal ions were not included in the buffers during purification. Binding of a second metal ion in the active site is observed in the presence of RNA¹¹. No EM density for divalent metal ions was observed in the Rat1 active site.

The Rail-Rtt103 interface

Rtt103 only has interactions with Rail in the current structure (Fig. 1b). Moreover, only a small segment of Rtt103 was observed to have good quality EM density, corresponding to residues 259–265 (Fig. 2a), even though full-length Rtt103 was in the sample. Approximately 550 Å² of the surface area of these residues are buried in the interface with Rail. Several additional residues at the N and C termini of this segment, corresponding to residues 255–258 and 266–270, have EM density in the map after heterogeneous refinement (Fig. 1d), which contribute 170 Å² of buried surface area to the interface. We have named this region of Rtt103 the Rail interaction segment (RIS), which follows the helical region of Rtt103 and is connected to it by a short linker (Fig. 1a). The rest of Rtt103, including the CID, has no observed EM density and is likely flexible in the current structure.

Residues 259–264 of the RIS adopt an extended conformation and form a parallel β-sheet with residues 17–19 (beginning of strand β2) of Rail (Fig. 2b). The side chains of Pro261 and Tyr263 of the Rtt103 RIS point toward Rail and contribute most to the interaction, burying 121 and 176 Å² of surface area, respectively. The Pro261 side chain is located in a hydrophobic pocket, formed by the side chains of Trp265, Phe269, Pro299, Cys313, Leu314 and Ile317 of Rail. The side chain of Tyr263 is flanked by Phe269 of Rail on one face and Gln20 and Pro21 on the other. The hydroxyl group of Tyr263 is hydrogen-bonded to the main-chain carbonyl oxygen of Phe269, with a distance of 2.8 Å. The side chains of RIS residues Ile259 and Ile260 are mostly on the surface, with that of Ile260 being in contact with Pro299 and Val300.

Residues 266–270 of Rtt103 contain three Asp and two Gly residues and are located next to a region of Rail that is highly enriched in Lys/Arg residues (Fig. 2c). In fact, residues 269–270 are at the beginning of a highly acidic segment in the sequence of *S. cerevisiae* Rtt103, with residues 269–287 being Asp residues (except Gly275 and Asn277). This highly negatively charged segment might have some favorable, though nonspecific, interactions with the positively charged surface patch of Rail. However, the interactions are likely to be weak, as residues 266–270 are not well ordered in the current structure (Fig. 1c).

Residues 260–264 are highly conserved among Rtt103 homologs among a collection of yeast species related to *S. cerevisiae* (Fig. 2d). Pro261 and Tyr263 are strictly conserved among these homologs, and residue 260 is hydrophobic (Leu, Ile, Phe). The stretch of electro-negative residues following the RIS is also seen in many of these

Table 1 | Cryo-EM data collection, structure refinement and validation statistics

Saccharomyces cerevisiae Rat1-Rail-Rtt103 complex	
Data collection and processing	
Magnification	105,000
Voltage (kV)	300
Electron exposure (e ⁻ /Å ²)	49.3
Defocus range (μm)	−0.6 to −2
Pixel size (Å)	0.413
Symmetry imposed	C1
Image stacks (no.)	6718
Initial particles images (no.)	3,614,995
Final particle images (no.)	552,608
Map resolution (Å)	2.85
FSC threshold	0.143
Map sharpening B-factor (Å ²)	−123
Refinement	
Number of protein residues	1115
Number of metal ions	1
Number of atoms	8975
R.m.s. deviations	
Bond lengths (Å)	0.004
Bond angles (°)	0.536
PDB validation	
Clash score	6
Poor rotamers (%)	0
Ramachandran plot	
Favored (%)	98.5
Allowed (%)	1.5
Disallowed (%)	0.0

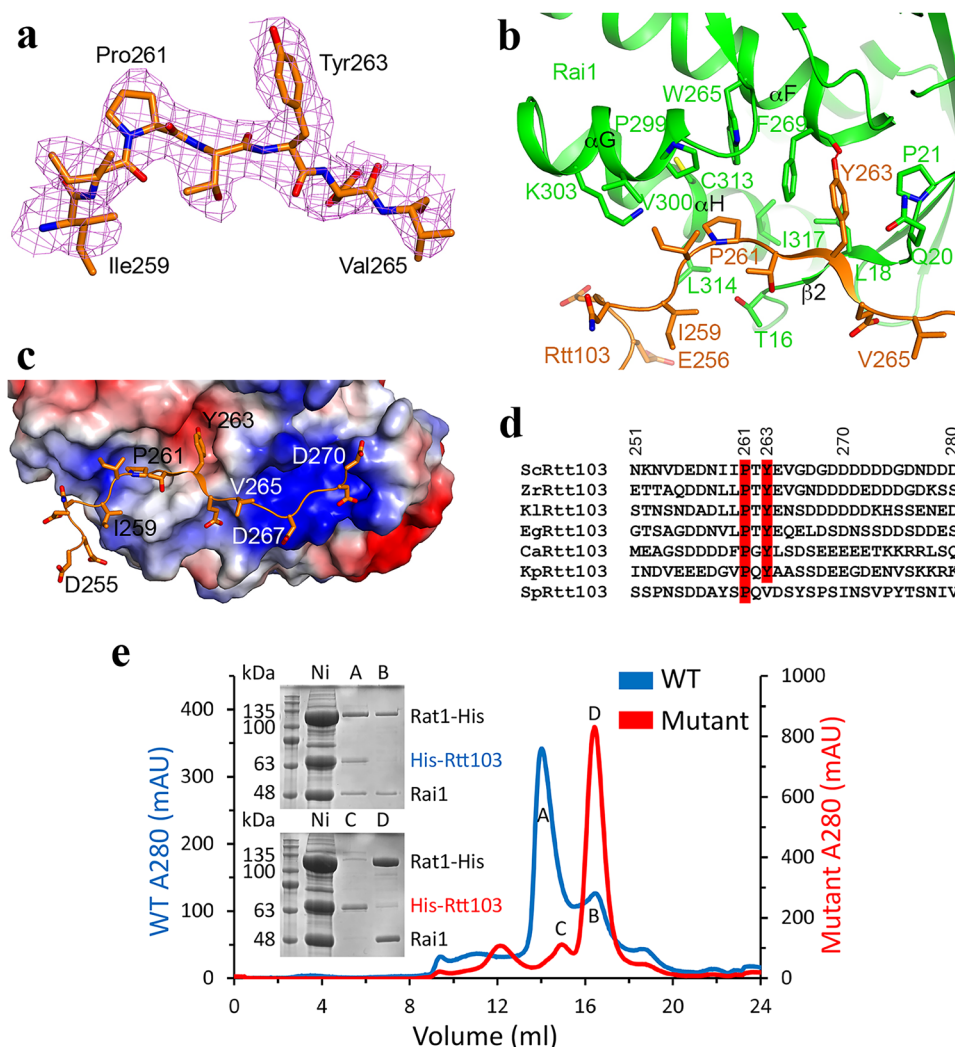


Fig. 2 | The Rai1-Rtt103 interface. **a** EM density of the segment of Rtt103 observed at high resolution in the current structure. **b** Detailed interactions between Rtt103 (orange) and Rai1 (green). **c** Electrostatic surface of Rai1 in the interface with Rtt103. A highly positive surface patch may interact with a stretch of negatively charged residues in Rtt103. Red: negatively charged; Blue: positively charged. **d** Sequence conservation of the Rai1 interaction segment (RIS) of Rtt103 homologs. Sc: *S. cerevisiae*; Zr: *Zygosaccharomyces rouxii*; Kl: *Kluyveromyces lactis*; Eg: *Eremothecium gossypii*; Ca: *Candida albicans*; Kp: *K. phaffii*; Sp: *S. pombe*. Residue numbers of *S. cerevisiae* Rtt103 are shown. Pro261 and Tyr263 are highlighted in

red. **e** Gel filtration profiles of wild-type Rtt103 co-expressed with Rai1-Rail (blue trace) and P261G/Y263A mutant of Rtt103 co-expressed with Rai1-Rail (red trace). Insets show SDS PAGE gels for peaks in the gel filtration profiles. Ni: eluates from the Ni column. Both Rai1 and Rtt103 carry a His tag. Peak A: Rai1-Rail-Rtt103 complex, B and D: Rai1-Rail complex; C: Rtt103 alone. Rtt103 alone runs larger than the Rai1-Rail complex on gel filtration, possibly due to the fact that it is mostly disordered or it forms aggregates. This experiment was done one time. Source data are provided as a Source Data file.

homologs. Rai1 residues in contact with the Rtt103 RIS are also highly conserved among these yeast species (Supplementary Fig. 2), suggesting that a similar Rai1-Rtt103 complex likely exists for these homologs.

However, Tyr263 is not conserved in the *S. pombe* Rtt103 homolog, and it is replaced by Val (Fig. 2d). This segment of *S. pombe* Rtt103 likely has much lower affinity for Rai1. Interestingly, both Pro261 and Tyr263 are conserved in *K. phaffii* Rtt103 (Fig. 2d), although this interaction was not observed in the reported structure (see below)¹⁶.

We next introduced mutations in the Rai1-Rtt103 interface to assess the structural observations. We generated the site-specific Rtt103 P261G/Y263A mutant, and co-expressed it with Rai1-Rail like for wild-type Rtt103. While a stable complex was observed on a gel filtration column with wild-type Rai1, Rai1 and Rtt103, only the Rai1-Rail complex was observed with the mutant Rtt103, even though it was expressed and could be pulled down with Ni affinity chromatography (Fig. 2e). The mutagenesis data confirm the structural observations

and demonstrate the importance of Pro261 and Tyr263 residues in the interactions between Rtt103 and Rai1.

To assess whether the RIS alone is sufficient to mediate the interaction with Rai1, we expressed and purified residues 243-272 of Rtt103 as an MBP fusion protein and carried out amylose resin pull-down experiments. The data showed that wild-type RIS could pull down purified Rai1-Rail complex, while the P261G/Y263A mutant RIS could not, even at a large excess (Supplementary Fig. 3). Therefore, the RIS is sufficient for the interaction between Rtt103 and Rai1-Rail.

Comparison to related structures

Structures of the *S. cerevisiae* Rai1-Rail complex together with RNA polymerase II (Pol II) were reported recently¹⁵. The overall structure of the Rai1-Rail complex is similar to that reported here, although several loops on the surface, especially in Rai1, have substantially different conformations (Fig. 3a). Rtt103 was not included in the protein expression in this other study. Strand β 1 and the beginning of strand β 2

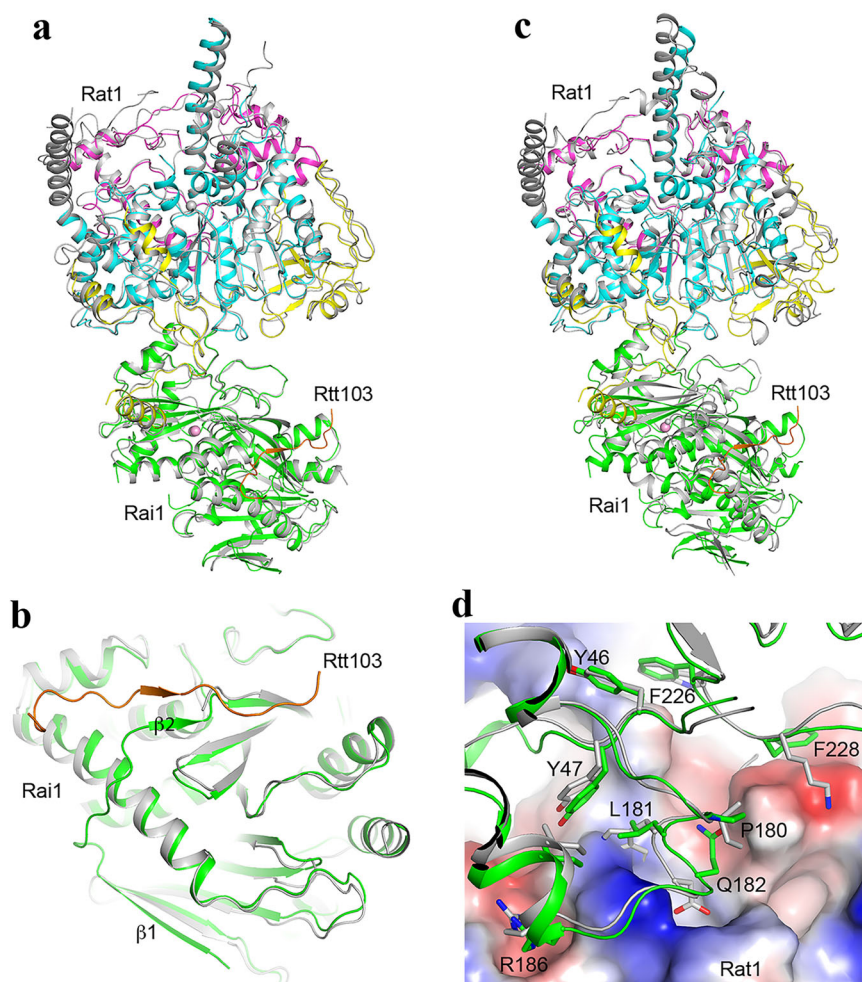


Fig. 3 | Comparisons to related structure. **a** Overlay of the *S. cerevisiae* Rat1-Rai1-Rtt103 ternary complex structure reported here (in color) and the *S. cerevisiae* Rat1-Rai1 binary complex structure together with Pol II (gray)¹⁵. The Pol II structure is not shown here for clarity, but shown in Supplementary Fig. 4. **b** Overlay of Rai1 in the Rtt103 binding region. Strands $\beta 1$ and $\beta 2$ of Rai1 in the Rat1-Rai1-Pol II complex are disordered, and the Rtt103 binding site does not exist. **c** Overlay of the *S. cerevisiae* Rat1-Rai1-Rtt103 ternary complex structure reported here (in

color) and the *S. pombe* Rat1-Rai1 binary complex structure (gray)⁹. **d** Detailed interactions in the Rat1-Rai1 interface. *S. cerevisiae* Rat1 is shown as an electrostatic surface, and Rai1 residues in the interface are shown as stick residues (green for *S. cerevisiae* Rai1 and gray for *S. pombe* Rai1). In all panels, the current structure of *S. cerevisiae* Rat1-Rai1-Rtt103 complex is shown in color, while previously published structures are in gray.

are disordered (Fig. 3b), suggesting that the Rtt103 binding site does not exist in this structure. On the other hand, an overlay of the Rat1-Rai1-Rtt103 structure reported here with that of the Rat1-Rai1-Pol II complex shows that the RIS binding site in Rai1 is accessible in the Pol II pre-termination transcription complex (Supplementary Fig. 4).

Structures of the yeast *Komagataella phaffii* Rat1-Rai1-Rtt103 complex, alone and together with Pol II, have also been reported¹⁶. The authors observed a hetero-tetramer of the Rat1-Rai1 complex, mediated by a Rat1 dimer. A single Rtt103 molecule is bound to this hetero-tetramer, with the CID primarily contacting one of the Rai1 molecules. Therefore, this mode of interaction between Rtt103 and Rai1 is entirely different from what we observed for the *S. cerevisiae* Rtt103-Rai1 complex, even though both Pro261 and Tyr263 of *S. cerevisiae* Rtt103 are conserved in *K. phaffii* Rtt103 (Fig. 2d). The CID is bound to the opposite face of Rai1, and the binding site for the RIS is available in this complex (Supplementary Fig. 5a). Moreover, the Rai1 binding site in the CID of *K. phaffii* Rtt103 overlaps with that for the Pol II CTD peptide²³ (Supplementary Fig. 5b), and therefore binding of Rai1 would be mutually exclusive with the binding of Pol II CTD in the *K. phaffii* complex. Further studies are needed to understand the molecular basis why the RIS in *K. phaffii* Rtt103 does not have a similar interaction with Rai1. We carried out an AlphaFold-

Multimer prediction^{24,25} for *K. phaffii* Rai1-Rtt103, which showed a similar complex as observed here for *S. cerevisiae* Rai1-Rtt103 (Supplementary Fig. 5c), while no contact was predicted with confidence between the Rtt103 CID and Rai1 (Supplementary Fig. 5d).

The Rat1 dimer observed in the *K. phaffii* Rat1-Rai1-Rtt103 complex is formed by residues poorly conserved among Rat1 homologs, a helix at the beginning of the linker between CR1 and CR2 and a helix in the C-terminal extension following CR2 (Supplementary Fig. 6a). Differences in amino acid side chains as well as main-chain conformations in this region may explain why *S. cerevisiae* Rat1 does not dimerize (Supplementary Fig. 6b). It should also be noted that *K. phaffii* Rat1 is a monomer in the complex with Pol II, similar to *S. cerevisiae* Rat1.

The overall structure of the *S. cerevisiae* Rat1-Rai1 complex is similar to that of the *S. pombe* Rat1-Rai1 complex reported earlier⁹. With the structures of Rat1 in overlay, only a 2.5° difference is observed for the orientation of Rai1 (Fig. 3c). One noticeable difference in the *S. cerevisiae* Rat1-Rai1 interface is that residues 893–935 of Rat1 are ordered, and the C-terminal part of this segment is in the Rai1 interface, which should provide additional stability for the Rat1-Rai1 complex. The equivalent residues were not included in the *S. pombe* Rat1 expression construct⁹, although this segment in *S. pombe* Rat1 does not appear to have any secondary structures. Moreover, an

AlphaFold2 prediction of the *S. pombe* Rat1-Rail complex did not show a similar feature as well. Therefore, this additional Rat1 segment in the Rail interface may be a feature unique to *S. cerevisiae* and closely related organisms.

Rail residues in the interface with Rat1 are generally conserved, or show conservative substitutions, between the *S. cerevisiae* and *S. pombe* homologs (Fig. 3d, Supplementary Fig. 2). Trp159 of *S. pombe* Rail is located in the center of the interface, and the W159A mutation can block Rat1-Rail interactions⁹. This residue is replaced by Leu181 in *S. cerevisiae* Rail, and in fact the conformation of Trp159 in *S. pombe* Rail could clash with *S. cerevisiae* Rat1 (Fig. 3d). Arg186 of *S. cerevisiae* Rail and its equivalent Arg164 of *S. pombe* Rail are both located in an electro-negative pocket on the surface of Rat1.

In summary, our structural studies have provided molecular insights into the *S. cerevisiae* Rat1-Rail-Rtt103 ternary complex, and the structural observations are confirmed by our mutagenesis studies. These results suggest a model where the Rtt103 CID positions this protein next to Pol II, and the Rtt103 RIS in turn helps to recruit Rat1-Rail to Pol II for termination in *S. cerevisiae*. Direct contacts between Pol II and Rat1^{15,16}, and likely other protein factors, also contribute to Pol II termination.

Methods

Protein expression and purification

Saccharomyces cerevisiae Rat1, Rail and Rtt103 were co-expressed in insect cells. N-terminal 6×His-tagged Rtt103 and untagged Rail (both full length) were cloned into the pFL vector. C-terminal 6×His-tagged Rat1 (residues 1-981) was cloned into the pFastBac438a vector²⁶. *Trichoplusia ni* (Tni) cells (Expression Systems 94-002S) were co-infected with both viruses at a cell density of 2×10^6 cells ml⁻¹ and harvested after 48 h.

For purification, the cells were lysed by sonication in a buffer containing 20 mM Tris (pH 8.0), 250 mM NaCl, 2 mM β-mercaptoethanol, 5% (v/v) glycerol, 0.1% Triton X-100. The cell lysate was then centrifuged at $15,000 \times g$ for 40 min at 4 °C. The protein complex was purified from the supernatant via nickel affinity chromatography (Qiagen). The elution was then purified with size exclusion chromatography using Superose 6 increase 10/300 column (Cytiva). Protein composition in the fractions were checked with SDS-PAGE. Fractions that contain the correct complex components were collected, concentrated and stored at -80 °C.

EM sample preparation and data collection

Specimens for cryo-EM analysis were prepared using a VitroBot plunge freezer (Thermo Scientific) in the Simons Electron Microscopy Center at the New York Structural Biology Center (NYSBC). 3.5 μl of the complex at 0.2 mg ml⁻¹ concentration was applied to an UltrAuFoil 300 mesh 1.2/1.3 grid (Quantifoil). The grid was blotted for 2 sec at 20 °C, 95% humidity and then plunged into liquid ethane. The quality of the grids was screened using a Glacios microscope (Thermo Scientific) at the Columbia University Cryo-Electron Microscopy Center.

6718 image stacks were collected using a Titan Krios electron microscope (Thermo Scientific) at the National Center for CryoEM Access and Training (NCCAT) at the NYSBC, equipped with a K3 direct electron detector (Gatan), with a total dose of 49.3 e⁻Å⁻² subdivided into 40 frames. The images were recorded at a nominal magnification of 105,000× and a calibrated pixel size of 0.413 Å, with a defocus range from -0.6 to -2 μm (Table 1).

Cryo-EM image processing, model building and refinement

Cryo-EM image processing was carried out using CryoSPARC²⁷. 3,614,995 particles were picked and subjected to 2D classification. After manually selection of the good 2D classes, 536,635 particles were used to generate an initial 3D volume, and rejected 2D classes were used to generate 3 junk volumes. The volumes were then used with all

particles for 3D heterogeneous refinement. After several rounds, 552,608 particles were subjected to non-uniform refinement, yielding a map at 2.85 Å resolution.

An initial model of the complex was generated with ColabFold²⁵. The ordered part of each protein was docked and fitted into the EM density using UCSF Chimera²⁸. Manual model building was carried out with Coot²⁹, and real-space refinement was carried out with PHENIX³⁰. The data processing and structure refinement statistics are summarized in Table 1.

Rat1-Rail-Rtt103 interactions

N-terminal 6×His-tagged Rtt103 wild-type was first cloned to pFastBac438b vector and the P261G/Y263A mutant was made with Gibson assembly and verified by sequencing. Both C-terminal 6×His-tagged Rat1 (residues 1-981) and Rail were cloned into pFastBac438a vector. Recombinant Rtt103 wild-type or mutant were co-expressed with Rat1-Rail and pulled down with Ni-NTA beads similarly as described above.

Analytical gel filtration experiments were carried out on a Superose 6 Increase 10/300 column, with a buffer containing 20 mM HEPES (pH 7.4) and 200 mM NaCl. Protein composition in each peak was examined with SDS PAGE.

N-terminal 6×His-MBP tagged *S. cerevisiae* Rtt103 RIS (243-272) wild-type or P261G/Y263A mutant was cloned into pET-28a vector and over-expressed in *E. coli* BL21(DE3) Rosetta cells (Novagen). Recombinant MBP-RIS fusion protein was purified with Ni-NTA and gel filtration (Superose 6 Increase 10/300) chromatography similarly as described above.

Purified Rat1-Rail complex was incubated with or without MBP-RIS fusion protein on ice for 30 min and then mixed with amylose beads for 1 h. The beads were then washed with 40 column volumes of buffer containing 20 mM HEPES and 100 mM NaCl. Proteins bound to amylose beads were eluted with SDS-PAGE loading dye and then checked with SDS-PAGE.

Reporting summary

Further information on research design is available in the Nature Portfolio Reporting Summary linked to this article.

Data availability

The structure of the *S. cerevisiae* Rat1-Rail-Rtt103 ternary complex has been deposited at the PDB under accession code [9DSO](#). The EM map has been deposited at the EMDB under accession code [EMD-47148](#). Source data are provided with this paper.

References

- Kim, M. et al. The yeast Rat1 exonuclease promotes transcription termination by RNA polymerase II. *Nature* **432**, 517–522 (2004).
- West, S., Gromak, N. & Proudfoot, N. J. Human 5'→3' exonuclease Xrn2 promotes transcription termination at co-transcriptional cleavage sites. *Nature* **432**, 522–525 (2004).
- Connelly, S. & Manley, J. L. A functional mRNA polyadenylation signal is required for transcription termination by RNA polymerase II. *Genes Dev.* **2**, 440–452 (1988).
- Luo, W., Johnson, A. W. & Bentley, D. L. The role of Rat1 in coupling mRNA 3'-end processing to transcription termination: implications for a unified allosteric-torpedo model. *Genes Dev.* **20**, 954–965 (2006).
- Proudfoot, N. J. Transcriptional termination in mammals: Stopping the RNA polymerase II juggernaut. *Science* **352**, aad9926 (2016).
- Eaton, J. D., Francis, L., Davidson, L. & West, S. A unified allosteric/torpedo mechanism for transcriptional termination on human protein-coding genes. *Genes Dev.* **34**, 132–145 (2020).
- Stevens, A. Purification and characterization of a *Saccharomyces cerevisiae* exoribonuclease which yields 5'-mononucleotides by a 5'→3' mode of hydrolysis. *J. Biol. Chem.* **255**, 3080–3085 (1980).

8. Xue, Y. et al. *Saccharomyces cerevisiae* Rai1 (YGL246c) is homologous to human DOM3Z and encodes a protein that binds the nuclear exoribonuclease Rat1p. *Mol. Cell. Biol.* **20**, 4006–4015 (2000).
9. Xiang, S. et al. Structure and function of the 5'→3' exoribonuclease Rat1 and its activating partner Rai1. *Nature* **458**, 784–788 (2009).
10. Jiao, X. et al. Identification of a quality-control mechanism for mRNA 5'-end capping. *Nature* **467**, 608–611 (2010).
11. Jiao, X., Chang, J. H., Kilic, T., Tong, L. & Kiledjian, M. A mammalian pre-mRNA 5' end capping quality control mechanism and an unexpected link of capping to pre-mRNA processing. *Mol. Cell* **50**, 104–115 (2013).
12. Jiao, X. et al. 5' end nicotinamide adenine dinucleotide cap in human cells promotes RNA decay through DXO-mediated deNADding. *Cell* **168**, 1015–1027 (2017).
13. Doamekpor, S. K., Sharma, S., Kiledjian, M. & Tong, L. Recent insights into noncanonical 5' capping and decapping of RNA. *J. Biol. Chem.* **298**, 102171 (2022).
14. Wang, V. Y., Jiao, X., Kiledjian, M. & Tong, L. Structural and biochemical studies of the distinct activity profiles of Rai1 enzymes. *Nucl. Acid Res.* **43**, 6596–6606 (2015).
15. Zeng, Y., Zhang, H. W., Wu, X. X. & Zhang, Y. Structural basis of exoribonuclease-mediated mRNA transcription termination. *Nature* **628**, 887–893 (2024).
16. Yanagisawa, T. et al. Structural basis of eukaryotic transcription termination by the Rat1 exonuclease complex. *Nat. Commun.* **15**, 7854 (2024).
17. Srividya, I., Tirupataiah, S. & Mishra, K. Yeast transcription termination factor Rtt103 functions in DNA damage response. *PLoS One* **7**, e31288 (2012).
18. Ramalingam, K. & Mishra, K. Transcription termination complex, Rtt103-Rai1-Rat1, regulates sub-telomeric transcripts in *Saccharomyces cerevisiae*. *RNA Biol.* **20**, 95–108 (2023).
19. Suh, H. et al. Direct Analysis of Phosphorylation Sites on the Rpb1 C-Terminal Domain of RNA Polymerase II. *Mol. Cell* **61**, 297–304 (2016).
20. Nemec, C. M. et al. Different phosphoisoforms of RNA polymerase II engage the Rtt103 termination factor in a structurally analogous manner. *Proc. Natl Acad. Sci. USA* **114**, E3944–e3953 (2017).
21. Jasnovidova, O., Krejčíková, M., Kubicek, K. & Stefl, R. Structural insight into recognition of phosphorylated threonine-4 of RNA polymerase II C-terminal domain by Rtt103p. *EMBO Rep.* **18**, 906–913 (2017).
22. Jasnovidova, O. et al. Structure and dynamics of the RNAPII CTDsome with Rtt103. *Proc. Natl Acad. Sci. USA* **114**, 11133–11138 (2017).
23. Lunde, B. M. et al. Cooperative interaction of transcription termination factors with the RNA polymerase II C-terminal domain. *Nat. Struct. Mol. Biol.* **17**, 1195–1201 (2010).
24. Evans, R. et al. Protein complex prediction with AlphaFold-Multimer. *bioRxiv*, <https://doi.org/10.1101/2021.10.04.463034> (2022).
25. Mirdita, M. et al. ColabFold: making protein folding accessible to all. *Nat. Methods* **19**, 679–682 (2022).
26. Gradia, S. D. et al. MacroBac: New Technologies for Robust and Efficient Large-Scale Production of Recombinant Multiprotein Complexes. *Methods Enzymol.* **592**, 1–26 (2017).
27. Punjani, A., Rubinstein, J. L., Fleet, D. J. & Brubaker, M. A. cryoSPARC: algorithms for rapid unsupervised cryo-EM structure determination. *Nat. Methods* **14**, 290–296 (2017).
28. Goddard, T. D., Huang, C. C. & Ferrin, T. E. Visualizing density maps with UCSF Chimera. *J. Struct. Biol.* **157**, 281–287 (2007).
29. Emsley, P. & Cowtan, K. D. Coot: model-building tools for molecular graphics. *Acta Cryst. D.* **60**, 2126–2132 (2004).
30. Liebschner, D. et al. Macromolecular structure determination using X-rays, neutrons and electrons: recent developments in Phenix. *Acta Crystallogr. D. Struct. Biol.* **75**, 861–877 (2019).

Acknowledgements

We thank the staff at the Columbia University Cryo-Electron Microscopy Center for help with screening EM grids, Alex Flynn and the staff at the NCCAT, NYSBC for help with cryo-EM data collection. This research is supported NIH grant R35GM118093 (to L.T.). Some of this work was performed at the National Center for CryoEM Access and Training (NCCAT) and the Simons Electron Microscopy Center located at the New York Structural Biology Center, supported by the NIH Common Fund Transformative High Resolution Cryo-Electron Microscopy program (U24 GM129539) and by grants from the Simons Foundation (SF349247) and NY State Assembly.

Author contributions

H.-F.C. conducted protein expression and purification, and cryo-EM experiments; H.-F.C. and L.T. conducted all structural analyses and wrote the manuscript.

Competing interests

The authors declare no competing interests.

Additional information

Supplementary information The online version contains supplementary material available at <https://doi.org/10.1038/s41467-025-58671-z>.

Correspondence and requests for materials should be addressed to Liang Tong.

Peer review information *Nature Communications* thanks Dong Wang and the other, anonymous, reviewers for their contribution to the peer review of this work. A peer review file is available.

Reprints and permissions information is available at <http://www.nature.com/reprints>

Publisher's note Springer Nature remains neutral with regard to jurisdictional claims in published maps and institutional affiliations.

Open Access This article is licensed under a Creative Commons Attribution-NonCommercial-NoDerivatives 4.0 International License, which permits any non-commercial use, sharing, distribution and reproduction in any medium or format, as long as you give appropriate credit to the original author(s) and the source, provide a link to the Creative Commons licence, and indicate if you modified the licensed material. You do not have permission under this licence to share adapted material derived from this article or parts of it. The images or other third party material in this article are included in the article's Creative Commons licence, unless indicated otherwise in a credit line to the material. If material is not included in the article's Creative Commons licence and your intended use is not permitted by statutory regulation or exceeds the permitted use, you will need to obtain permission directly from the copyright holder. To view a copy of this licence, visit <http://creativecommons.org/licenses/by-nc-nd/4.0/>.

© The Author(s) 2025